International Journal of Pharmaceutics 583 (2020) 119375

Contents lists available at ScienceDirect

International Journal of Pharmaceutics

journal homepage: www.elsevier.com/locate/ijpharm

Preparation and characterization of parthenolide nanocrystals for enhancing therapeutic effects of sorafenib against advanced hepatocellular carcinoma

Pan Liang[a], Hangyi Wu[a], Zhenhai Zhang[b], Shulong Jiang[c,*], Huixia Lv[a,*]

[a] Department of Pharmaceutics, State Key Laboratory of Natural Medicines, China Pharmaceutical University, Nanjing 211198, China
[b] Jiangsu Province Academy of Traditional Chinese Medicine, Nanjing 210023, China
[c] Clinical Medical Laboratory Center, Jining No. 1 People's Hospital, Jining, Shandong 272000, China

ARTICLE INFO

Keywords:
Parthenolide
Nanocrystals
Sorafenib
Hepatocellular carcinoma
Combination therapy

ABSTRACT

A novel nanocrystals delivery system of parthenolide (PTL) was designed to combined application with sorafenib (Sora) for advanced hepatocellular carcinoma (HCC) therapy, attempting to not only improve the poor aqueous solubility of PTL, but also enhance the synergistic therapeutic effects with Sora. The PTL nanocrystals (PTL-NCs) were prepared by precipitation-high-pressure homogenization method. The formed PTL-NCs with rod morphology possessed size of 126.9 ± 2.31 nm, zeta potential of −11.18 ± 0.59 mV and drug loading of 31.11 ± 1.99%. Meanwhile, PTL in PTL-NCs exhibited excellent storage stability and sustained release behavior. The combination therapy of Sora and PTL-NCs (Sora/PTL-NCs) *in vitro* for HepG2 cells presented superior therapeutic effects over that of individual PTL and Sora on intracellular uptake, cell proliferation inhibition and migration inhibition. Meanwhile the strongest anti-tumor effect with 81.86% inhibition rate and minimized systemic toxicity of Sora/PTL-NCs *in vivo* were obtained on tumor-bearing mice compared with that of PTL (48.84%) and Sora (58.83%). Thus, these findings suggested that PTL-NCs as an effective delivery system for the synergistically used with Sora to gain an optimal response against HCC, for referenced in the industrialization of nanocrystals products for intravenous administration.

1. Introduction

Hepatocellular carcinoma (HCC) is a highly malignant tumor, which leads increased cancer mortality due to its early metastasis, poor prognosis and tumor heterogeneity (Zhang et al., 2018). HCC has risen to be the fifth commonest cancer and second cause of cancer death, with 5-year survival rates below 5% (In Rae Cho et al., 2017; Walker et al., 2019). Until now, surgical excision supplemented with chemotherapy remains the major treatment for advanced HCC (Jiang et al., 2018; Yu et al., 2014). However, poor selectivity and efficacy of chemotherapeutic drugs may be accompanied by serious side effects, resulting in unsatisfactory treatments (Shi et al., 2012). Hence, it is an urgent need for developing systemic strategies against HCC with high efficacy and low toxicity.

Currently, Sorafenib (Sora), an oral multi-kinase inhibitor, is firstly approved by FDA in 2005 for advanced HCC treatment (Xu and Zheng, 2017). Sora can reduce tumor angiogenesis and induce tumor cell apoptosis by inhibiting vascular endothelial growth factor (VEGF) (Llovet, 2008). However, recent clinical reports demonstrated that HCC displayed drug resistance to single antiangiogenic therapy due to overexpressed nuclear factor-κB (NF-κB) (Han et al., 2017). NF-κB plays a critical role in the proliferation and invasion of HepG2 cells as well as the expression of invasion-related molecules (Wu et al., 2009). Recently, the effective combination therapy of Sora with chemotherapy agents such as paclitaxel (Lei et al., 2019) and rapamycin (Wang et al., 2008) were investigated. These combination therapies could increase tumor cellular sensitivity to chemotherapy agents and thus enhance their anti-tumor efficacy. However, the co-delivery system was extremely limited on giving and adjusting proper dose, as well as maintaining their stability, due to the different physiochemical properties of the cooperators (Gill et al., 2012; Liu et al., 2012; Meng et al., 2013).

It has been reported that the combination of Sora and NF-κB inhibitors showed synergistic antitumor activity (Abdulghani et al., 2016; Hikita et al., 2010). Several nature products with no major side effects were investigated to exhibit antitumor effects via inhibiting NF-κB signaling pathway, including parthenolide (Sohma et al., 2011), curcumin (Qiao et al., 2012) and artemisinin (Zhu et al., 2012). Parthenolide (PTL) is an active compound responsible for the anti-inflammatory therapy (Zhang et al., 2004), which was first found in feverfew in 1990 (Groenewegen, 1990). Moreover, PTL has shown its

* Corresponding author.
E-mail addresses: jnsljiang@163.com (S. Jiang), lvhuixia@163.com (H. Lv).

https://doi.org/10.1016/j.ijpharm.2020.119375
Received 29 November 2019; Received in revised form 21 February 2020; Accepted 23 April 2020
Available online 25 April 2020
0378-5173/

potential to inhibit tumor cell proliferation, especially HepG2 cell line (Carlisi et al., 2011; Kim et al., 2013; Lesiak et al., 2010; Sun et al., 2014). The antitumor mechanism of PTL were played through inducing autophagy and apoptosis as well as inhibiting angiogenesis (Sun et al., 2014). In addition, PTL can also act by sensitizing tumor cells to conventional chemotherapy drugs such as paclitaxel and vinorelbine (Liu et al., 2008; Patel, 2000). Therefore, the combination therapy of PTL and Sora may be exploited as an additional therapy effect. However, the clinical value of PTL was hindered due to its poor aqueous solubility and low oral bioavailability (Taleghani et al., 2017). Furthermore, the gastrointestinal side effects caused by oral administration of PTL have been identified in the Phase I trial (Eardie and Christy Yoder, 2004). Therefore, it would be essential to develop formulations used in other administration routes of PTL to overcome above drawbacks.

Nanotechnologies, including micelles (Watkins, 2011), nanoparticles (Zong et al., 2015) and liposomes (Jin et al., 2018), have drawn many attentions in their abilities to improve undesired solubility of insoluble drugs. However, low drug loading, poor stability, and toxicity of excessive additives still limit their industrial production and clinical application (Zhang et al., 2011). Nanocrystals (NCs) were considered as a novel carrier-free nanoparticle strategy for enhancing the water solubility of drugs since its excellent drug loading capacity, simplicity in production and common applicability (Junyaprasert, 2015; Mishra and Srivalli, 2015). Additionally, NCs could not only protect drugs from degradation and prolong their circulation time (Gao et al., 2010), but also realize the sustained release and target to the specific tissues or organs (Huang et al., 2010; Lin et al., 2014). An unignorable superiority of the NCs is that they could be applied in various administration routes including oral, intravenous and transdermal administration and transformed into various dosage forms such as tablets, capsules and so on (Lei et al., 2013). Meanwhile, several drug nanocrystals products for oral formulations are already commercial available owing to above advantages (Van Eerdenbrugh et al., 2008). However, it is also remained challenges for the nanocrystals used in parenteral administration to take into the markets as a result of their instability during storage and application (Sun and Yeo, 2012).

Poloxamer 188 (F68), a nonionic surfactant, is widely used as stabilizer of nanosuspensions since its steric stabilization effect on avoiding the aggregation of nano-particles. More interestingly, studies have shown that F68 can interact with drug-resistant tumors to enhance tumor sensitivity of chemotherapeutic drugs. This phenomenon is related to the molecules size and hydrophilic lipophilic balance (HLB) value of the poloxamer (Moghimi, 2000). Lecithin acts as a natural ampholytic surfactant, which is considered a good excipient to enhance physical stability of drug delivery systems such as liposomes and nanoparticles (Hafner et al., 2009). This collaboration can possess both electrostatic and steric interaction to prevent particle aggregation during the homogenization progress, having a better effectiveness in stabilization. Herein, the PTL-NCs for intravenous administration were prepared using lecithin and F68 as stabilizers by precipitation-high-pressure homogenization method (PHPH). The combined therapeutic effects of PTL-NCs with Sora against HCC were investigated, including *in vitro* cell cytotoxicity, cell uptake, cell migration and *in vivo* antitumor assays of tumor-bearing nude mice.

2. Materials and methods

2.1. Materials

Parthenolide was provided by Ruifensi biology (Chengdu, China). Sorafenib tosylate was obtained from Dalian Meilun Biotechnology Co. Ltd. Poloxamer 188 was obtained from BASF Co. Ltd (Mannheim, Germany). Lecithin was purchased from A.V.T Shanghai pharmaceutical Co. Ltd. DMEM high glucose medium, phosphate buffer (PBS) and trypsin with 0.25% EDTA were purchased from Jiangsu KeyGEN BioTECH Co. Ltd (Nanjing, China) and fetal bovine serum (FBS) was provided by GIBCO (USA) Life Technologies. 5-diphenyl-tetrazolium bromide (MTT) was provided by Dalian Meilun Biotechnology Co. Ltd. All the other reagents were analytical or chromatography grade and used without further purification.

2.2. Cells and animals

HepG2 cell lines were obtained from the cell bank of Chinese Academy of Sciences and cultured in DMEM high glucose medium at 37 °C in an atmosphere containing 5% CO_2. The female BALB/c nude mice (five weeks old) were purchased from Nanjing Cavans Biotech Co. Ltd. The nude mice were kept with specific-pathogen free (SPF) cleanliness level at a room temperature of 25 ± 2 °C and a relative humidity of 50 ± 10%. Animal welfare and experimental procedures were strictly in accordance with the Guide for the Care and Use of Laboratory Animals and the related ethics regulations of China Pharmaceutical University. Animal protocols were reviewed and approved by the Internal Animal Care and Use Committee of China Pharmaceutical University.

2.3. Preparation and characterization of the nanocrystals

The nanocrystals were prepared by precipitation and high-pressure homogenization method (PHPH). In brief, the organic phase was prepared by dissolving PTL (120 mg) in ethanol (10 mL) and stirred until dissolved completely. Meanwhile, appropriate amount F68 and lecithin (1:2, w/w) were dissolved in 48 mL of water to obtain the aqueous phase. The organic phase was added into the aqueous phase under stirred continuously. After that, the solution was evaporated at 40 °C to remove organic solvents. The crude nanocrystals were homogenized respectively for 10, 15, 20, 30, 40 cycles with 500, 700, 1000 bar pressure through high pressure homogenizer (ATS Industrial Systems Co. Ltd).

The mean diameter, zeta potential and polydispersity index (PDI) of the PTL-NCs were determined by dynamic light scattering (DLS) (Malvern Company, England). The morphology of the PTL-NCs was visualized by transmission electron microscope (TEM, Hitachi TEM system).The PTL concentration and the drug loading (DL) in PTL-NCs were determined by high performance liquid chromatography (HPLC) (Shimadzu, HT-2010C) performed on Hedera ODS-2 C18 column with mobile phase of acetonitrile-water (60/40, v/v) at flow rate of 1.0 mL/min. The detection wavelength and column temperature were 210 nm and 25 °C, respectively. The sample volume injected was 20 μL.

2.4. In vitro release

The release of nanocrystals *in vitro* was evaluated by dialysis method. In brief, the prepared fresh nanocrystals (1 mL) and PTL suspension (obtained by directly dispersing free PTL drug in pure water) were placed in a dialysis bag (MWCO: 3500). Then the dialysis bag was immersed in 40 mL phosphate buffer (pH = 7.4) release medium containing 0.8% (w/v) sodium dodecyl sulfate (SDS) and placed in a shaker with a speed of 100 rpm at 37 °C. During the study, 1 mL sample was collected at certain time intervals (0.25, 0.5, 1, 2, 4, 6, 8, 10, 12, 24, 36, 48, 60, 72 h), while an equivalent volume fresh release medium was supplemented immediately to maintain the sink condition. The collected sample was filtered by 0.22 μm millipore filters before HPLC determination. The experiment was performed in triplicate.

2.5. Stability of the nanocrystals

The PTL-NCs were lyophilized and reconstituted respectively with deionized water at 0, 7, 14, 30, 60 and 90 days to investigate freeze-drying stability. In addition, the storage stability of the PTL-NCs was investigated at 4 °C. The particle size and PDI were measured using DLS at 0, 2, 4, 6, 8, 10, 15, 30, 60 and 90 days, respectively. The PTL

concentration of the PTL-NCs and the freeze-dried PTL-NCs were detected at 0, 7, 14, 30, 60 and 90 days.

Considering the further *in vitro* and *in vivo* study, it was required to determine the dilution stability. Detailly, the PTL-NCs were diluted with DMEM complete medium into 10, 20, 50 and 100 times to detect particle size and PDI.

2.6. Intracellular uptake quantification

For *in vitro* cellular uptake quantification assays, HepG2 cells were seeded into 6-well plates at the density of 5×10^4 and incubated for 24 h at 37 °C. Then, the medium was removed and washed twice before added following samples incubated for 4 h: (1) PTL (2.5, 5, 10 μM), (2) PTL-NCs (2.5, 5, 10 μM), (3) Sora/PTL (10 μM/10 μM), (4) Sora/PTL-NCs (10 μM/10 μM). After incubation, the cells were washed twice with PBS to remove free drugs and fixed with 500 μL deionized water to lyse cell with repeated freeze–thaw method. The intracellular drug content was determined through HPLC analysis of above item 2.3. Protein contents were quantified by a BCA assay kit (Jiangsu KeyGEN BioTECH Co. Ltd).

2.7. Cellular proliferation inhibition

The methylthiazol tetrazolium (MTT) assay was used to test anti-tumor activity of the PTL-NCs. Briefly, HepG2 cells were seeded in 96-well plates and treated with different concentration of Sora (2.5, 5, 7.5, 10, 12.5, 15, 17.5 μM), PTL (10, 20, 40, 80, 100, 160, 200 μM), PTL-NCs (the equivalent of PTL 10, 20, 40, 80, 100, 160, 200 μM), Sora/PTL (2:1, 1:1, 1:2, 1:4, 1:8), Sora/PTL-NCs (2:1, 1:1, 1:2, 1:4, 1:8) for 24 h. After that, the cells were incubated with 20 μL MTT (5 mg/mL) for 4 h to crystallize. After removing the pre-incubation solution, 150 μL DMSO were added to each well, shaking until the formazan crystals were dissolved completely. The absorbance (Abs) was measured at 490 nm by microplate reader (MK-3, Thermo, USA) and the cell viability was calculated by Eq. (1). Combination index (CI) was used for the quantitative analysis of combined therapeutic effects of PTL-NCs and Sora. As theory of Chou-Talalay defined (Tang et al., 2018), CI $>$ 1 for antagonism, CI $=$ 1 for additive effect and CI $<$ 1 for synergism. Besides, the synergistic effects were inversely proportional to the CI values. The CI value in combined therapy of Sora and PTL was calculated by Eq. (2):

$$\text{Cell viability } \% = [(A_M - A_B)/(A_C - A_B)] \times 100\% \quad (1)$$

where A_M, A_C and A_B were defined as the absorbance of drug treated group, control group and blank group, respectively.

$$CI = \frac{(D)\text{Sora}}{(D_{50})\text{Sora}} + \frac{(D)\text{PTL}}{(D_{50})\text{PTL}} \quad (2)$$

where (D) Sora and (D) PTL were the concentration of Sora and PTL used in combined therapy to achieve 50% inhibitory effects, (D_{50}) Sora and (D_{50}) PTL were the concentration of Sora and PTL to achieve the same effects individually.

2.8. Cell migration

To evaluate ability to migration of HepG2 cells, they were seeded in 6-well plate with 5×10^5 cells per well overnight. The cells were washed twice mildly with PBS, then were incubated with each sample as follow for 24 h, (1) Blank DMEM medium, (2) PTL (2.5 μM), (3) PTL-NCs (2.5 μM), (4) Sora (2.5 μM), (5) Sora/PTL (2.5 μM/2.5 μM), (6) Sora/PTL-NCs (2.5 μM/2.5 μM). Images were captured at 0 h and 24 h. Image J software (NIH, Bethesda, MA, USA) was used to calculate scratch area. The Eq. (3) was used to calculate the healing rate (in triplicate).

$$\text{Healing rate } \% = (W_0 - W_1)/W_0 \times 100\% \quad (3)$$

where W_0 and W_1 were defined as the scratch area at 0 h and 24 h, respectively.

2.9. In vivo anti-tumor efficacy

2.9.1. Anti-tumor efficacy

HepG2 cells (about 6×10^6 cells) were injected into the right armpit of the female BALB/c nude mice to obtain tumor-bearing nude mice. When the volume of tumors reached 100 mm^3, nude mice were divided randomly into six groups (five mice per group) to give each of the following samples, (1) Saline, (2) PTL (iv every two days, 12 mg/kg), (3) PTL-NCs (iv every two days, 12 mg/kg), (4) Sora (oral every day, 30 mg/kg), (5) Sora (oral every day, 30 mg/kg)/PTL (iv every two days, 12 mg/kg), (6) Sora (oral every day, 30 mg/kg)/PTL-NCs (iv every two days, 12 mg/kg). During the experiment, the survival states of the mice (activity, sleep, tortuosity and death) were observed. Tumor volume and body weight of nude mice were monitored every two days during 15-day treatment. At the end of the experiment, the animals were sacrificed by cervical dislocation. The subcutaneous metastatic tumor and major organs were completely excised, weighed and used for the pathological examination of HE staining and Ki-67 staining. The tumor volume (V) and the tumor inhibition rate (TIR) were calculated by Eqs. (4) and (5), respectively.

$$V = 0.5 \times \text{length} \times \text{wide}^2 \quad (4)$$

$$TIR = [(W_C - W_E)/W_C] \times 100\% \quad (5)$$

where W_E and W_C were defined as the tumor weight of the experiment group and control group.

The body decrease rate (BDR) was calculated as Eq. (6).

$$BDR = [(W_F - W_I)/W_F] \times 100\% \quad (6)$$

where W_I and W_F were defined as the initial body weight and final body weight.

2.9.2. HE staining

The tumor and the organs (including heart, liver, spleen, lung and kidney) of nude mice were excised and fixed with 4% paraformaldehyde at least 24 h. After that, they were performed for HE staining after embedded and made into pathological sections, which were further observed and imaged under the microscope (Nikon Corporation Tokyo, Japan).

2.9.3. Ki-67 staining

Ki-67, a marker of cell proliferation, was discovered by the reactivity of rabbit antiserum raised against the Hodgkin's lymphoma cell line L428 (GERDE, 1983). To evaluate the tumor cell proliferation, all stained slices were performed for Ki-67 staining and further observed imaged under the microscope. The images were analyzed with Image J software. Three 200 × fields view per slice per group were randomly selected to calculate positive rate of Ki-67.

2.10. Statistical analysis

The results were expressed as mean ± standard deviation (SD). The independent Sample's T test with SPSS 19.0 (SPSS Inc., Chicago, IL) was used to evaluate the data between two groups. p value of $<$ 0.05 was considered as statistical significance.

3. Results and discussions

3.1. Preparation and characterization of the nanocrystals

The PTL-NCs were successfully prepared by PHPH method. In our study, lecithin and F68 were employed as the stabilizers with the 2:1 ratio of lecithin to F68. The lecithin and F68 diffused rapidly and

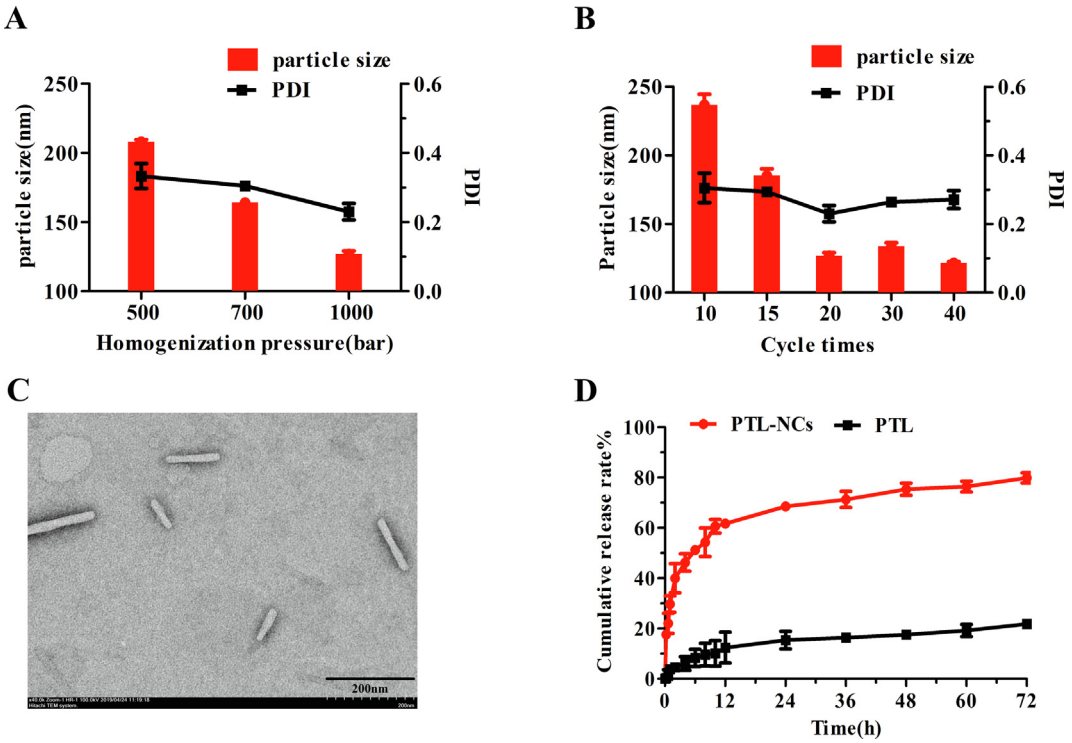

Fig. 1. The influence of (A) the pressure and (B) the cycle times of homogenization on particle size and PDI of the PTL-NCs. (C) The TEM images of the PTL-NCs. (D) The PTL release profile of PTL-NCs in PBS (pH = 7.4) at 37 °C. Data are presented as mean ± SD (n = 3).

covered the surface of the crystals during homogenization progress, which can gather the advantages of both steric and electrostatic stabilization for achieving an efficient particle size reduction and stored stability of PTL. The characteristics of PTL-NCs were shown in Fig. 1. In addition, our results showed that the particle size and PDI of the PTL-NCs were significantly influenced by the pressure and cycle times of homogenization. The particle size decreased from 208.2 nm to 126.9 nm and the PDI decreased from 0.333 to 0.230 when the homogenization pressure increased from 500 bar to 1000 bar (Fig. 1A). According to the homogenization theory, higher-velocity fluid in the homogenizer gap caused by higher pressure, leading to generation of more gas bubbles eventually to break the microcrystals into nanocrystals (Karadag et al., 2014). However, it seemed that continuous increase on cycle times after 20 resulted in the fluctuation of particles size and PDI, which might be due to a slightly reversible formation of aggregates that were disaggregated in the next cycles (Mishra et al., 2009) (Fig. 1B). Thus, 1000 bar and 20 times were considered as optimal pressure and cycle times of homogenization to achieve the minimized particle size and PDI.

Furthermore, DLS analysis and TEM images were performed to characterize both the size distribution and morphology of PTL-NCs. The PTL-NCs were possessed as rod morphology with a size of 126.9 ± 2.31 nm and 0.230 ± 0.024 PDI, indicating that the obtained NCs were small and well dispersed. The zeta potential of NCs was −11.18 ± 0.59 mV. The TEM images showed lager size of NCs could be related to the crystal growth after dried according to Ostwald ripening (Sharma et al., 2015), compared to DLS analysis (Fig. 1C). Meanwhile, the drug loading of 31.11 ± 1.99% of the PTL-NCs were achieved.

3.2. In vitro release

The release property of PTL from the PTL-NCs was evaluated by dialysis bag method. As shown in Fig. 1D, the results showed that the cumulative release amount of free PTL was only about 15% at 12 h and 20% at 72 h. While, PTL-NCs showed an appropriate release rate with a dramatically rapid release about 65% at 12 h and 80% release at 72 h. The appropriate drug release rate of the PTL-NCs could maintain a relatively stable blood concentration during intravenous administration, avoiding excessive peak-to-valley efficacy and adverse effects of treatment. The release profile of the PTL-NCs was defined as a two-phase release: previously burst release and subsequently sustained release. The previously burst release could be attributed to smaller particle size and lager specific surface area of PTL-NCs, compared with PTL (Koopaei et al., 2012). And the subsequently sustained release might be contributed to enhance antitumor effects during long-term therapy (He et al., 2015).

3.3. Stability of the nanocrystals

As shown in Fig. 2A, the particle size was around 140 nm after lyophilization and the PDI was less than 0.292 for three months' storage. It was reported that freeze-dried nanocrystals could minimize the shortage of aggregation problem, providing the extra stability (Anup et al., 2018). As shown in Fig. 2B, the particle size and PDI were changed negligibly after the PTL-NCs was diluted to 10, 20, 50 and 100 times by DMEM complete medium. This indicated that PTL-NCs could be available during intravenous infusion. By contrast, the storage stability of the PTL-NCs solution was unsatisfactory. Its particle size was increased about 50 nm and the PDI was slightly increased to 0.265 during three months at 4 °C (Fig. 2C). Furthermore, we detected the PTL concentration from PTL-NCs solution and freeze-dried PTL-NCs powder after 90 days storage. The results showed that the PTL concentration was decreased from 2.262 mg/mL to 1.998 mg/mL in PTL-NCs solution, while it was changed negligibly in freeze-dried PTL-NCs (Fig. 2D). Thus, the final form should be an important factor for PTL-NCs storage.

3.4. Intracellular uptake quantification

The intracellular uptake of Sora, PTL and PTL-NCs was evaluated by BCA protein quantification. As shown in Fig. 3A, the intracellular drug content was significantly enhanced by PTL-NCs compared to free PTL,

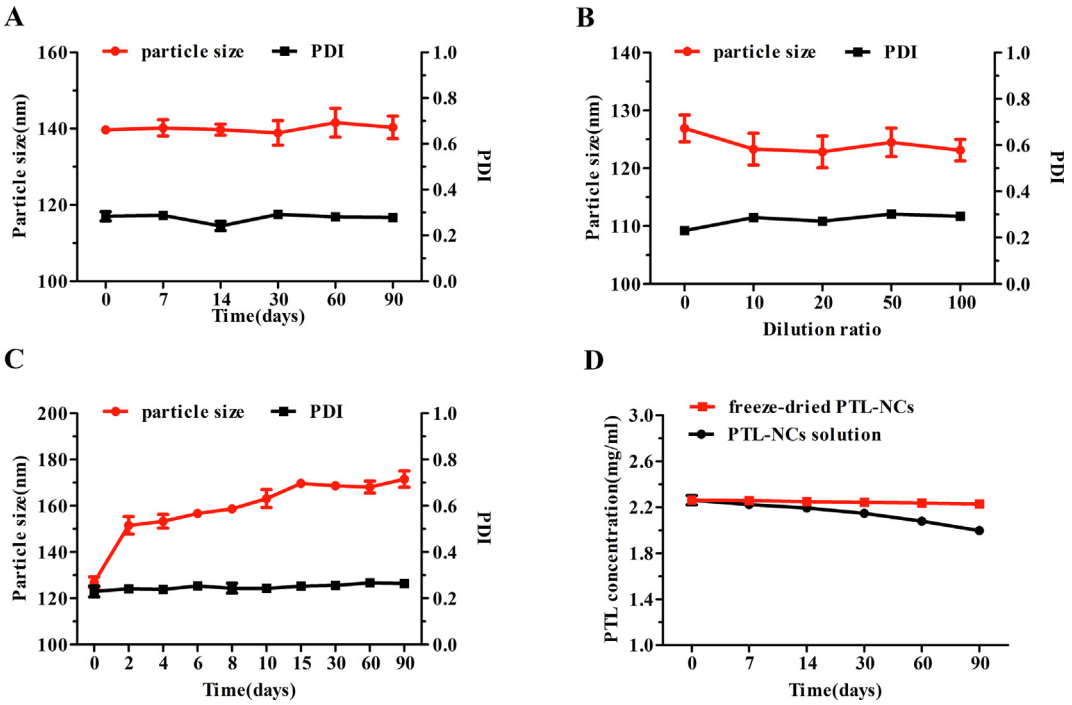

Fig. 2. The particle size and PDI of the PTL-NCs after (A) lyophilization, (B) dilution, (C) storage at 4 ˚C. (D) The PTL concentration of the PTL-NCs solution and freeze-dried PTL-NCs during a 90-day's storage. Data are presented as mean ± SD (n = 3).

when the feeding concentration of PTL arrived at 10 μM, indicating that the form of NCs as drug carrier could promote the internalization of PTL. While, there was no significant difference between PTL and PTL-NCs at 2.5 μM and 5 μM. This might because that the internalization pathway of NCs was altered from passive diffusion to endocytosis as the drug concentration upregulated. Based on these results, the combined concentration of Sora and PTL-NCs was selected at 10 μM, respectively. After incubation for 4 h, compared to Sora, the intracellular uptake of Sora treated with Sora/PTL and Sora/PTL-NCs were statistically increased (Fig. 3B), which might be due to the inhibition of P-glycoprotein efflux by PTL (Dajun Liu et al., 2013). According to Fig. 3C, the intracellular PTL content of Sora/PTL-NCs group was nearly twice that of Sora/PTL group, which was consistent with the results of the single treatment with PTL and PTL-NCs. Thus, the PTL-NCs served as a high-efficiency drug delivery system not only exhibited superior cell uptake activity, but also enhanced the intracellular uptake of Sora.

3.5. *In vitro* antiproliferation

The *in vitro* antiproliferation activity of PTL-NCs was investigated through MTT assay. As Fig. 4A shown, the inhibitory effects of PTL and PTL-NCs were increased with PTL concentration. The half-maximal inhibitory concentration (IC_{50}) of PTL and PTL-NCs were 50.891 and 33.618 μM, respectively, suggesting that the PTL-NCs exhibited better antiproliferation activity compared to PTL on HepG2 cells. These might be related to the nanocrystal structure of the PTL-NCs, which were internalized via endocytosis rather than passive diffusion, leading to better cytotoxicity than that of PTL (Miao et al., 2016).

The combined therapeutic effects of Sora and PTL-NCs were also characterized by MTT assay. As illustrated in Fig. 4B, 4C, after incubation for 24 h, all treatments displayed dose-dependent cytotoxicity, especially the combinations of Sora and PTL-NCs gave rise to increased inhibitory effects. Sora/PTL-NCs showed significantly higher inhibitory effects on HepG2 cells in comparison to Sora/PTL, indicating that PTL-NCs exhibited better combined therapeutic effects with Sora *in vitro*. This might be attributed to the delayed release of the drug from NCs system (Shi et al., 2019). As theory of Chou-Talalay defined (Chou, 1983), the CI values of Sora/PTL-NCs at molar ratios of 1:8, 1:4, 1:2, 1:1 and 2:1 were 1.033, 0.855, 0.637, 0.346 and 0.495, respectively, which were slightly lower than that of Sora/PTL (1.146, 0.922, 0.853, 0.480 and 0.583) (Fig. 4D). These data intuitively indicated that the *in vitro* synergistic antitumor effects of Sora/PTL-NCs with lower CI values at

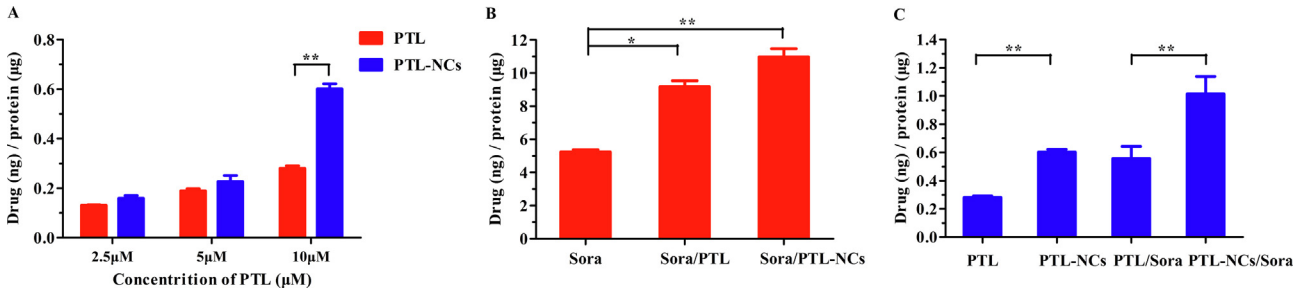

Fig. 3. The intracellular uptake drug content of different groups was evaluated by the ratio of drug (ng)/protein (μg). (A) The PTL content in HepG2 cells in the treatment of PTL and PTL-NCs at 2.5 μM, 5 μM and 10 μM, respectively. (B) The intracellular Sora content and (C) the intracellular PTL content in HepG2 cells in the treatment of Sora (10 μM), PTL (10 μM), PTL-NCs (10 μM), Sora/PTL (10 μM/10 μM) and Sora/PTL-NCs (10 μM/10 μM). Data are presented as mean ± SD (n = 3). * means $p < 0.05$, ** means $p < 0.01$.

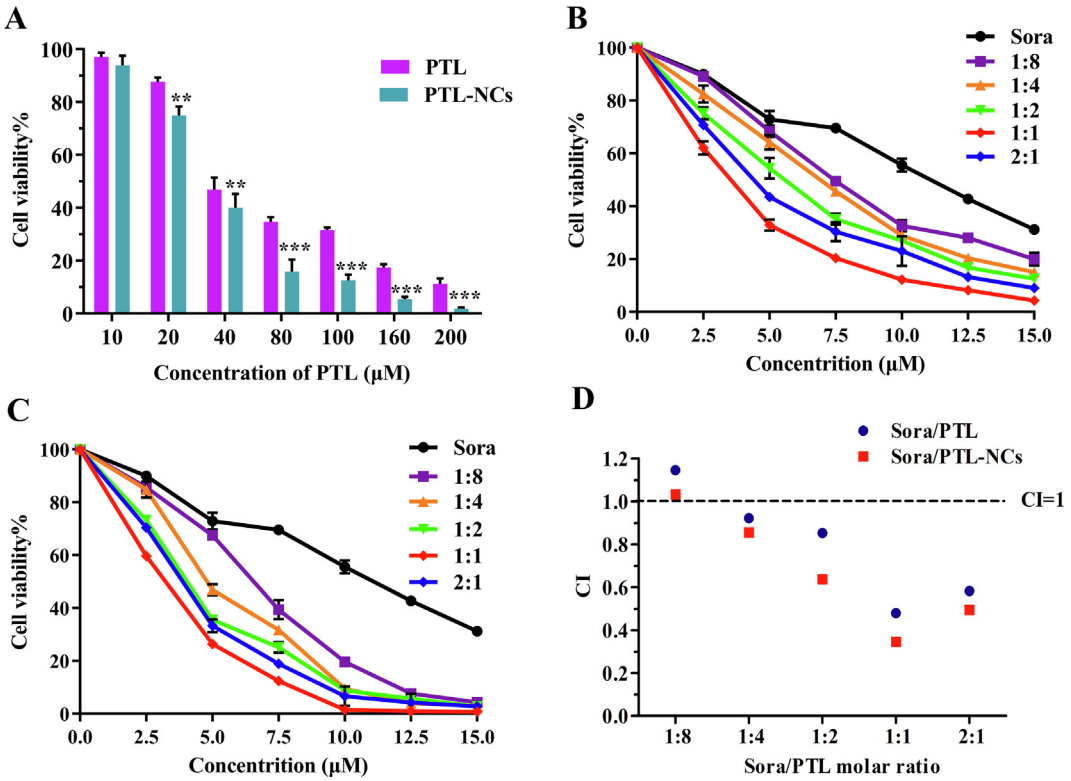

Fig. 4. (A) The *in vitro* antiproliferation activity of PTL and PTL-NCs, variable molar ratios of Sora to (B) PTL and (C) PTL-NCs in HepG2 cells after incubation for 24 h. (D) The CI value of Sora and PTL combinations at different molar ratios. Data are presented as mean ± SD (n = 6). * means $p < 0.05$, ** means $p < 0.01$ and *** means $p < 0.001$.

same molar ratio were stronger, compared with Sora/PTL, which were consisted with previous results. Contacted with the the intracellular uptake results, the accumulation of Sora in cells were enhanced by the combination with PTL, but it did not mean that the inhibitory effects on HepG2 cells were always increased with PTL ratio. This could be explained that the slightly antagonistic interaction between PTL and Sora were exhibited as the intracellular drugs contents reached to a certain concentration (Lifen Deng et al., 2013; Pawaskar et al., 2013). Herein, to achieve a maximized synergistic effect, the combination of Sora and PTL with a molar ratio of 1:1 was chosen as optimal regimen for further study.

3.6. Cell migration

The ability of Sora, PTL, PTL-NCs, Sora/PTL and Sora/PTL-NCs to impede HepG2 cell migration were tested through the wound healing assays. As shown in Fig. 5A, the control group (blank DMEM medium) performed strongest migration ability with the healing rate of 82.21%, while PTL-NCs and Sora groups exhibited a certain antimigration activity. Compared to control group, the treatments of Sora/PTL-NCs on HepG2 cells showed the most efficient migration inhibitory activity with the weakest healing rate of 27.04%. It suggested that PTL-NCs was effective in the suppression of HepG2 cells migration. Meanwhile, the strong synergistic effects were achieved through combined application of Sora and PTL-NCs.

3.7. In vivo anti-tumor efficacy

The HepG2 cell subcutaneous tumor-bearing nude mice model was used to assess *in vivo* anti-tumor assays. As presented in Fig. 6A, the tumor volume of nude mice treated with saline were increased rapidly over time. Despite the tumor growth of PTL group was slightly inhibited, no statistically difference was observed between PTL groups and saline group. This might be related to poor accumulation of free PTL in tumors via passive diffusion (Maedaa and Daruwalla, 2009). However, after intravenous injection of PTL-NCs, the tumor growth exhibited significant inhibition rate of 48.84%. The possible explanation of this behavior could be that the small size of NCs about 100 nm was favorable for passively targeting to the tumor site via the enhanced permeability (Sarbari and Sahoo, 2011). Meanwhile, the nude mice treated with Sora performed 58.83% tumor inhibition rate. Remarkably, the nude mice treated with Sora/PTL-NCs showed strongest inhibition rate with 81.86%, resulting in the smallest tumor volume and tumor weight after 15-day treatment (Fig. 6C). The relative tumor inhibition rate of the treatment with Sora/PTL-NCs was increased about 23% compared to Sora alone.

The body weight change of nude mice was considered as an important indicator to evaluate the toxicity of different treatments. As illustrated in Fig. 6B, the body weight of PTL and PTL-NCs changed negligibly, suggesting no obvious systemic toxicity. Despite the final body weight of nude mice treated with Sora, Sora/PTL and Sora/PTL-NCs decreased slightly, compared to saline group, there were no significant difference for Sora ($p = 0.214$), Sora/PTL ($p = 0.163$) and Sora/PTL-NCs ($p = 0.312$). Moreover, HE staining of major organs of nude mice were shown in Fig. 6E. Almost all visceral tissues with different treatments performed similar morphological characteristics, suggesting the low system toxicity at the test dose. Additionally, as shown in Fig. 6F, the HE staining of tumor tissues treated with saline showed normal morphological characteristics with no cell necrosis, indicating vigorous growth of tumor cells. In contrast, tumor tissues of nude mice with treatments of Sora, PTL-NCs and Sora/PTL-NCs exhibited a certain degree of tumor cell reduction and necrosis, especially that of Sora/PTL-NCs. Furthermore, the Ki-67 protein, a human nuclear antigen only expressed in the G 1, S and G 2 phases of the cell cycle, used as a cell proliferation indicator (Schmilovitz-Weiss, 2011). The Ki-67 positive cells in the Sora/PTL-NCs with positive rate of

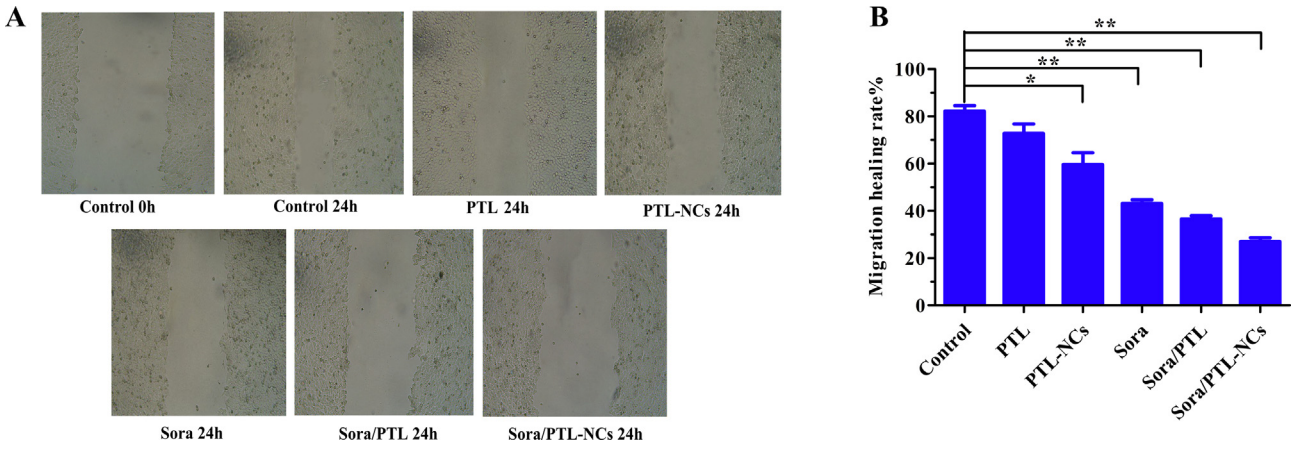

Fig. 5. (A) The antimigration activity of different treatments in HepG2 cells after incubated for 24 h. (B) The migration healing rate of different treatments in HepG2 cells after incubated for 24 h. Data are presented as mean ± SD (n = 3). * means p < 0.05, ** means p < 0.01.

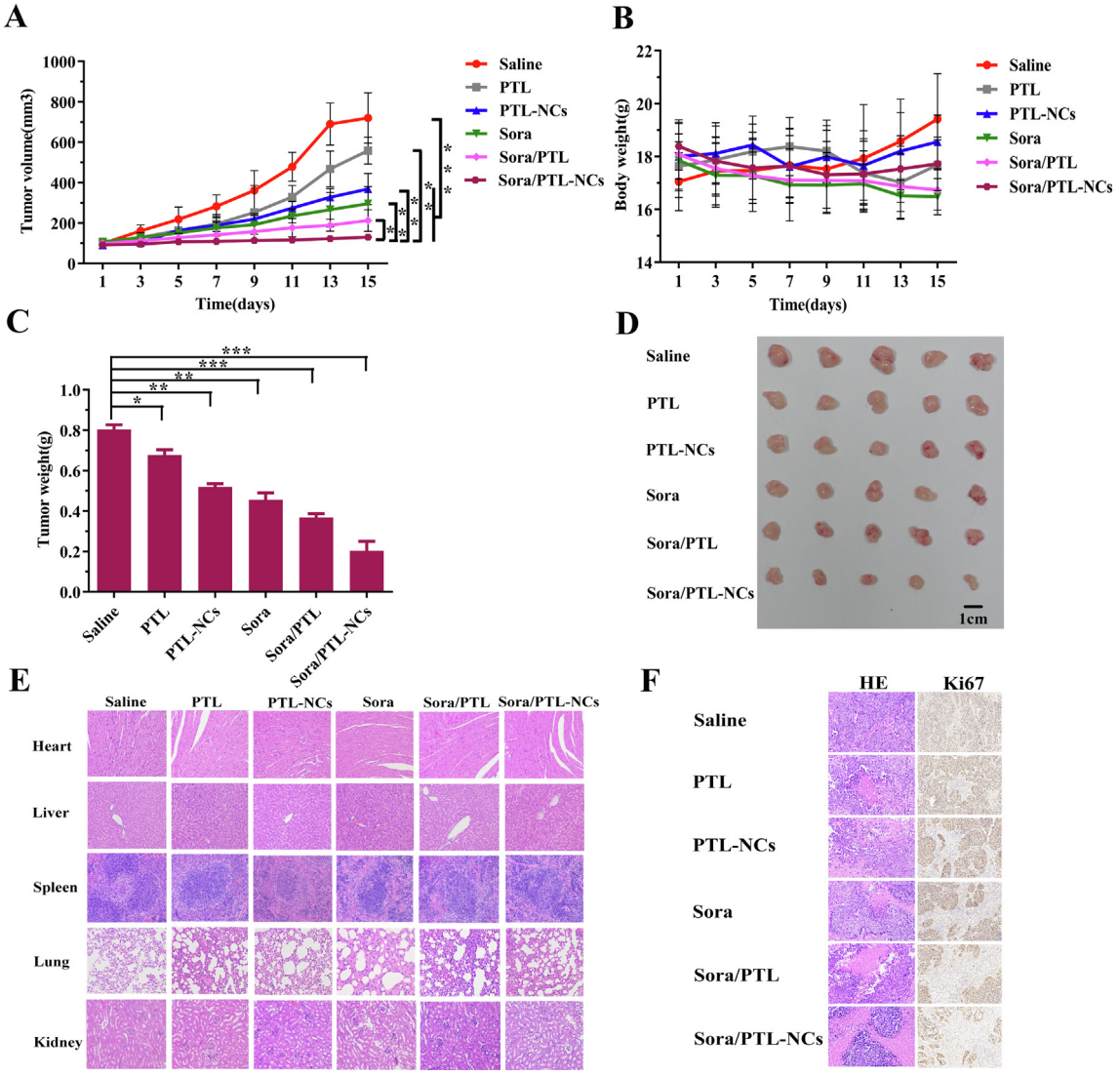

Fig. 6. *In vivo* therapeutic effects of different treatments on HepG2 tumor-bearing nude mice model. (A) Tumor volume, (B) Body weight, (C) Average weight and (D) images of excised tumors at day 15. (E) The HE staining images of major organs of tumor-bearing nude mice in response to different treatments at day 15 (200×). (F) The histological analysis of tumor slices after HE staining and Ki-67 staining in response to different treatments at day 15 (200×). Data are presented as mean ± SD (n = 5). * means $p < 0.05$, ** means $p < 0.01$ and *** means $p < 0.001$.

7.69 ± 1.05% was notably less than saline group (46.58 ± 1.36%), indicating significantly inhibited proliferation of tumor cells after treatment. Hence, Sora/PTL-NCs achieved its synergistic combination therapy via inhibition of tumor cells proliferation and induction of tumor cells necrosis *in vivo*, which was compatible with the *in vitro* studies. Based on the reported data, the oral bioavailability of Sora in female mice was about 78.6%, which might mean almost complete absorption (Liu et al., 2016). Contacted with the results of MTT assay, the combination therapy of Sora and PTL-NCs with the molar ratio of 1:1 showed strongest inhibitory effects to HepG2 cells, but the ratio of 1:2 with CI value less 1 (CI = 0.637) also exhibited good synergistic activity. Therefore, to keep the synergistic effects *in vivo*, it could be supposed that the molar ratio of two drugs at tumor site might be within 1:2–1:1.

The combined administrations at a 1:1 M ratio of Sora to PTL-NCs have proved to be effectively inhibited tumor growth, but it remains to been verified whether this is the optimal combination regimen for clinical trial. In preclinical tumor models, the administered dose of sorafenib (30 mg/kg) equivalents to *in vitro* concentrations of 4.2 μM, which is less than 30% of therapeutic dose in human patients (Shacham-Shmueli et al., 2012). Of significant note, for the higher dose accompanied by more obvious toxicity, it did not mean that the patients treated with the higher dose at the same dose molar ratio were more appropriate than lower dose during clinical treatment (Blanco et al., 2014). Therefore, both pharmacokinetics and pharmacodynamics assays of the combined regimens with various molar ratios may need to be performed simultaneously. In addition, to increase clinical feasibility of combination therapy, we will design administration groups with high, median and low dose at the same dose molar ratio in follow-up experiments. To sum up, the combination therapy of Sora with oral administration and PTL-NCs with intravenous administration was effective for enhancing anti-tumor efficacy without toxicity on major organs, which was the first attempt to enhance the antitumor efficacy of Sora. Furthermore, to achieve better drug compliance and synergistic antitumor efficacy, we are trying to investigate the combined oral therapy, especially the PTL-NCs with different particle sizes combined with Sora to reduce the gastrointestinal response and enhance the absorption of PTL.

4. Conclusion

In summary, a PTL-NCs formulation was developed for the combination therapy with Sora to treat HCC. The PTL-NCs was beneficial for tumor passive target via small uniform size about 100 nm, and it exhibited high dilution stability and storage stability, especially stored after lyophilization. Furthermore, *in vitro* release profile confirmed that PTL-NCs could provide the sustained release of PTL, contributing to enhance therapeutic effects through prolonged treatment time. It was worth noting that Sora/PTL-NCs exhibited superior synergistic intracellular uptake, cell proliferation inhibition and migration inhibition against HCC *in vitro*. *In vivo* anti-tumor studies revealed that the Sora/PTL-NCs with tumor inhibition rate by 81.86% performed excellent synergistic therapeutic effects compared to that of sole Sora and PTL. Moreover, a minimized systemic toxicity was observed on tumor-bearing mice treated with Sora/PTL-NCs. Herein, the PTL-NCs with high biosecurity may not only provide a strategy for the combination therapy with Sora to enhance synergistic anti-tumor effects, but also develop a reference for the drug nanocrystals applied in intravenous administration to realize industrial production.

CRediT authorship contribution statement

Pan Liang: Conceptualization, Methodology, Formal analysis, Investigation, Visualization, Writing - original draft. **Hangyi Wu:** Conceptualization, Formal analysis, Investigation, Visualization, Writing - original draft. **Zhenhai Zhang:** Conceptualization, Methodology, Formal analysis, Investigation, Visualization, Investigation, Writing - review & editing. **Shulong Jiang:** Conceptualization, Resources, Supervision, Project administration, Software, Validation, Writing - review & editing. **Huixia Lv:** Conceptualization, Data curation, Formal analysis, Funding acquisition, Investigation, Supervision, Visualization, Writing - original draft, Writing - review & editing.

Declaration of Competing Interest

The authors declare that they have no known competing financial interests or personal relationships that could have appeared to influence the work reported in this paper.

Acknowledgements

This work was financially supported by the National Natural Science Foundation of China (81673830), six talent peaks project of Jiangsu Province (YY053), Major Project and Double first-class innovative team (CPU2018GY28) and National Science and Technology Major Project (2017zx09101001005). This work was also supported in part by the National Natural Science Foundation of China (grant no. 81873249) and the Natural Science Foundation of Shandong Province (grant. no. ZR2019MH058).

References

Abdulghani, J., Gokare, P., Gallant, J.N., Dicker, D., Whitcomb, T., Cooper, T., Liao, J., Derr, J., Liu, J., Goldenberg, D., Finnberg, N.K., El-Deiry, W.S., 2016. Sorafenib and Quinacrine Target Anti-Apoptotic Protein MCL1: A Poor Prognostic Marker in Anaplastic Thyroid Cancer (ATC). Clin. Cancer Res. 22, 6192–6203.

Anup, N., Thakkar, S., Misra, M., 2018. Formulation of olanzapine nanosuspension based orally disintegrating tablets (ODT); comparative evaluation of lyophilization and electrospraying process as solidification techniques. Adv. Powder Technol. 29, 1913–1924.

Blanco, E., Sangai, T., Wu, S., Hsiao, A., Ruiz-Esparza, G.U., Gonzalez-Delgado, C.A., Cara, F.E., Granados-Principal, S., Evans, K.W., Akcakanat, A., Wang, Y., Do, K.A., Meric-Bernstam, F., Ferrari, M., 2014. Colocalized delivery of rapamycin and paclitaxel to tumors enhances synergistic targeting of the PI3K/Akt/mTOR pathway. Mol. Ther. 22, 1310–1319.

Carlisi, D., D'Anneo, A., Angileri, L., Lauricella, M., Emanuele, S., Santulli, A., Vento, R., Tesoriere, G., 2011. Parthenolide sensitizes hepatocellular carcinoma cells to TRAIL by inducing the expression of death receptors through inhibition of STAT3 activation. J. Cell. Physiol. 226, 1632–1641.

Chou, T.-C., 1983. Analysis of combined drug effects: a new look at a very old problem, 450–454.

Dajun Liu, Y.L., Liu, Minghua, Ran, Limei, Li, Yan, 2013. Reversing resistance of multi-drug-resistant hepatic carcinoma cells with parthenolide. Future Oncol. 9, 595–604.

Eardie III, A. Curry, Christy Yoder, D.J.M., 2004. Phase I dose escalation trial of feverfew with standardized doses of parthenolide in patients with cancer. Invest. New Drugs 22, 299–305.

Gao, Y., Li, Z., Sun, M., Li, H., Guo, C., Cui, J., Li, A., Cao, F., Xi, Y., Lou, H., Zhai, G., 2010. Preparation, characterization, pharmacokinetics, and tissue distribution of curcumin nanosuspension with TPGS as stabilizer. Drug Dev. Ind. Pharm. 36, 1225–1234.

Gerde, J., 1983. Production of a mouse monoclonal antibody reactive with a human nuclear antigen associated with cell proliferation. Znt. J. Cancer 31, 13–20.

Gill, K.K., Kaddoumi, A., Nazzal, S., 2012. Mixed micelles of PEG(2000)-DSPE and vitamin-E TPGS for concurrent delivery of paclitaxel and parthenolide: enhanced chemosenstization and antitumor efficacy against non-small cell lung cancer (NSCLC) cell lines. Eur. J. Pharm. Sci. 46, 64–71.

Groenewegen, 1990. A comparison of the effects of an extract of feverfew and parthenolide, a component of feverfew, on human platelet activity in-vitro. J. Pharm. Pharmacol. 42, 553–557.

Hafner, A., Lovrić, J., Voinovich, D., Filipović-Grčić, J., 2009. Melatonin-loaded lecithin/chitosan nanoparticles: Physicochemical characterisation and permeability through Caco-2 cell monolayers. Int. J. Pharm. 381, 205–213.

Han, P., Li, H., Jiang, X., Zhai, B., Tan, G., Zhao, D., Qiao, H., Liu, B., Jiang, H., Sun, X., 2017. Dual inhibition of Akt and c-Met as a second-line therapy following acquired resistance to sorafenib in hepatocellular carcinoma cells. Mol. Oncol. 11, 320–334.

He, W., Lv, Y., Zhao, Y., Xu, C., Jin, Z., Qin, C., Yin, L., 2015. Core–shell structured gel-nanocarriers for sustained drug release and enhanced antitumor effect. Int. J. Pharm. 484, 163–171.

Hikita, H., Takehara, T., Shimizu, S., Kodama, T., Shigekawa, M., Iwase, K., Hosui, A., Miyagi, T., Tatsumi, T., Ishida, H., 2010. The Bcl-xL inhibitor, ABT-737, efficiently induces apoptosis and suppresses growth of hepatoma cells in combination with sorafenib. Hepatology 52, 1310–1321.

Huang, X., Peng, X., Wang, Y., Wang, Y., Nie, S., 2010. A Reexamination of Active and Passive Tumor Targeting by Using Rod-Shaped Gold Nanocrystals and Covalently Conjugated Peptide Ligands. ACS Nano 4, 5887–5896.

In Rae Cho, H.W.L., Ki Jun Song, Beom Kyung Kim, 2017. Conditional survival estimate in patients with barcelona clinic liver cancer stage B/C hepatocellular carcinoma treated with hepatic arterial infusion chemotherapy with/without concurrent radiotherapy. Oncotarget 8, 79914-79926.

Jiang, S., Li, M., Hu, Y., Zhang, Z., Lv, H., 2018. Multifunctional self-assembled micelles of galactosamine-hyaluronic acid-vitamin E succinate for targeting delivery of norcantharidin to hepatic carcinoma. Carbohydr. Polym. 197, 194–203.

Jin, X., Zhou, J., Zhang, Z., Lv, H., 2018. The combined administration of parthenolide and ginsenoside CK in long circulation liposomes with targeted tLyp-1 ligand induce mitochondria-mediated lung cancer apoptosis. Artif. Cells Nanomed. Biotechnol. 46, S931–S942.

Josep M. Llovet, M., 2008. Sorafenib in Advanced Hepatocellular Carcinoma. N. Engl. J. Med. 378–390.

Junyaprasert, V.B., 2015. Nanocrystals for enhancement of oral bioavailability. Asian J. Pharmaceut. 13–23.

Karadag, A., Ozcelik, B., Huang, Q., 2014. Quercetin nanosuspensions produced by high-pressure homogenization. J. Agric. Food Chem. 62, 1852–1859.

Kim, S.-L., Kim, S.H., Trang, K.T.T., Kim, I.H., Lee, S.-O., Lee, S.T., Kim, D.G., Kang, S.-B., Kim, S.-W., 2013. Synergistic antitumor effect of 5-fluorouracil in combination with parthenolide in human colorectal cancer. Cancer Lett. 335, 479–486.

Koopaei, M.N., Maghazei, M.S., Mostafavi, S.H., Jamalifar, H., Dinarvand, R., 2012. Enhanced Antibacterial Activity of Roxithromycin Loaded Pegylated Poly Lactide-co-glycolide Nanoparticles. DARU J. Pharmaceut. Sci. 20, 92.

Lei, G., Liu, G., Ma, J., Wang, X., Zhou, L., Li, X., Wang, F., 2013. Application of Drug Nanocrystal Technologies on Oral Drug Delivery of Poorly Soluble Drugs. Pharm. Res. 30, 307–324.

Lei, M., Ma, G., Sha, S., Wang, X., Feng, H., Zhu, Y., Du, X., 2019. Dual-functionalized liposome by co-delivery of paclitaxel with sorafenib for synergistic antitumor efficacy and reversion of multidrug resistance. Drug Deliv 26, 262–272.

Lesiak, K., Koprowska, K., Zalesna, I., Nejc, D., Düchler, M., Czyz, M., 2010. Parthenolide, a sesquiterpene lactone from the medical herb feverfew, shows anticancer activity against human melanoma cells in vitro. Melanoma Res. 20, 21–34.

Lifen Deng, Z.R., Jia, Qingan, Wu, Weizhong, 2013. Schedule-dependent antitumor effects of 5-fluorouracil combined with sorafenib in hepatocellular carcinoma. BMC Cancer 13.

Lin, Z., Gao, W., Hu, H., Ma, K., He, B., Dai, W., Wang, X., Wang, J., Zhang, X., Zhang, Q., 2014. Novel thermo-sensitive hydrogel system with paclitaxel nanocrystals: High drug-loading, sustained drug release and extended local retention guaranteeing better efficacy and lower toxicity. J. Control. Release 174, 161–170.

Liu, C., Chen, Z., Chen, Y., Lu, J., Li, Y., Wang, S., Wu, G., Qian, F., 2016. Improving Oral Bioavailability of Sorafenib by Optimizing the “Spring” and “Parachute” Based on Molecular Interaction Mechanisms. Mol. Pharm. 13, 599–608.

Liu, S., Guo, Y., Huang, R., Li, J., Huang, S., Kuang, Y., Han, L., Jiang, C., 2012. Gene and doxorubicin co-delivery system for targeting therapy of glioma. Biomaterials 33, 4907–4916.

Liu, Y., Lu, W.L., Guo, J., Du, J., Li, T., Wu, J.W., Wang, G.L., Wang, J.C., Zhang, X., Zhang, Q., 2008. A potential target associated with both cancer and cancer stem cells: a combination therapy for eradication of breast cancer using vinorelbine stealthy liposomes plus parthenolide stealthy liposomes. J. Control. Release 129, 18–25.

Maedaa, H., Daruwalla, J., 2009. Polymeric drugs for efficient tumor-targeted drug delivery based on EPR-effect. Eur. J. Pharm. Biopharm. 71, 409–419.

Meng, H., Mai, W.X., Zhang, H., Xue, M., Xia, T., Lin, S., Wang, X., Zhao, Y., Ji, Z., Zink, J.I., 2013. Codelivery of an optimal drug/siRNA combination using mesoporous silica nanoparticles to overcome drug resistance in breast cancer in vitro and in vivo. ACS Nano 7, 994–1005.

Miao, X., Li, Y., Wang, X., Lee, S.M., Zheng, Y., 2016. Transport Mechanism of Coumarin 6 Nanocrystals with Two Particle Sizes in MDCKII Monolayer and Larval Zebrafish. ACS Appl. Mater. Interfaces 8, 12620–12630.

Mishra, B., Srivalli, K.M.R., 2015. Drug Nanocrystals: Four Basic Prerequisites for Formulation Development and Scale-Up. Curr. Drug Targets 16, 136–147.

Mishra, P.R., Al Shaal, L., Muller, R.H., Keck, C.M., 2009. Production and characterization of Hesperetin nanosuspensions for dermal delivery. Int. J. Pharm. 371, 182–189.

Moghimi, S.M., 2000. Poloxamers and poloxamines in nanoparticle engineering and experimental medicine. Trends Biotechnol. 18, 412–420.

Patel, N.M., 2000. Paclitaxel sensitivity of breast cancer cells with constitutively active NF-kB is enhanced by IkBa super-repressor and parthenolide. Oncogene 19, 4159–4169.

Pawaskar, D.K., Straubinger, R.M., Fetterly, G.J., Ma, W.W., Jusko, W.J., 2013. Interactions of everolimus and sorafenib in pancreatic cancer cells. AAPS J. 15, 78–84.

Qiao, Q., Jiang, Y., Li, G., 2012. Curcumin improves the antitumor effect of X-ray irradiation by blocking the NF-κB pathway. Anticancer Drugs 23, 597–605.

Sarbari, A., Sahoo, S.K., 2011. PLGA nanoparticles containing various anticancer agents and tumour delivery by EPR effect. Adv. Drug Deliv. Rev. 63, 170–183.

Schmilovitz-Weiss, H., 2011. Tissue expression of squamous cellular carcinoma antigen and Ki-67 in hepatocellular carcinoma-correlation with prognosis: A historical prospective study. Diagn. Pathol. 6, 121.

Shacham-Shmueli, E., Geva, R., Figer, A., Bulocinic, S., Nalbandyan, K., Shpigel, S., Atsmon, J., Brendel, E., 2012. Phase I trial of sorafenib in combination with 5-fluorouracil/leucovorin in advanced solid tumors. J. Clin. Pharmacol. 52, 656–669.

Sharma, S., Verma, A., Teja, B.V., Shukla, P., Mishra, P.R., 2015. Development of stabilized Paclitaxel nanocrystals: In-vitro and in-vivo efficacy studies. Eur. J. Pharm. Sci. 69, 51–60.

Shi, K., Xue, B., Jia, Y., Yuan, L., Han, R., Yang, F., Peng, J., Qian, Z., 2019. Sustained co-delivery of gemcitabine and cis-platinum via biodegradable thermo-sensitive hydrogel for synergistic combination therapy of pancreatic cancer. Nano Res. 12, 1389–1399.

Shi, L., Tang, C., Yin, C., 2012. Glycyrrhizin-modified O-carboxymethyl chitosan nanoparticles as drug vehicles targeting hepatocellular carcinoma. Biomaterials 33, 7594–7604.

Sohma, I., Fujiwara, Y., Sugita, Y., Yoshioka, A., Shirakawa, M., Moon, J., Takiguchi, S., Miyata, H., Yamasaki, M., Mori, M., 2011. Parthenolide, An NF-κB Inhibitor, Suppresses Tumor Growth and Enhances Response to Chemotherapy in Gastric Cancer. 8, 39.

Sun, B., Yeo, Y., 2012. Nanocrystals for the parenteral delivery of poorly water-soluble drugs. Curr. Opin. Solid State Mater. Sci. 16, 295–301.

Sun, J., Zhang, C., Bao, Y.L., Wu, Y., Chen, Z.L., Yu, C.L., Huang, Y.X., Sun, Y., Zheng, L.H., Wang, X., Li, Y.X., 2014. Parthenolide-induced apoptosis, autophagy and suppression of proliferation in HepG2 cells. Asian Pac. J. Cancer Prev. 15, 4897–4902.

Taleghani, A., Nasseri, M.A., Iranshahi, M., 2017. Synthesis of dual-action parthenolide prodrugs as potent anticancer agents. Bioorg. Chem. 71, 128–134.

Tang, P., Sun, Q., Yang, H., Tang, B., Pu, H., Li, H., 2018. Honokiol nanoparticles based on epigallocatechin gallate functionalized chitin to enhance therapeutic effects against liver cancer. Int. J. Pharm. 545, 74–83.

Van Eerdenbrugh, B., Van den Mooter, G., Augustijns, P., 2008. Top-down production of drug nanocrystals: nanosuspension stabilization, miniaturization and transformation into solid products. Int. J. Pharm. 364, 64–75.

Walker, S., Wankell, M., Ho, V., White, R., Deo, N., Devine, C., Dewdney, B., Bhathal, P., Govaere, O., Roskams, T., Qiao, L., George, J., Hebbard, L., 2019. Targeting mTOR and Src restricts hepatocellular carcinoma growth in a novel murine liver cancer model. PLoS ONE 14, e0212860.

Wang, Z., Zhou, J., Fan, J., Qiu, S.J., Yu, Y., Huang, X.W., Tang, Z.Y., 2008. Effect of rapamycin alone and in combination with sorafenib in an orthotopic model of human hepatocellular carcinoma. Clin. Cancer Res. 14, 5124–5130.

Watkins, H.C., 2011. Novel Parthenolide Delivery System for Cancer Treatment IEEE Annual Northeast Bioengineering Conference (NEBEC) 37.

Wu, J.M., Sheng, H., Saxena, R., Skill, N.J., Bhat-Nakshatri, P., Yu, M., Nakshatri, H., Maluccio, M.A., 2009. NF-kappaB inhibition in human hepatocellular carcinoma and its potential as adjunct to sorafenib based therapy. Cancer Lett. 278, 145–155.

Xu, J., Zheng, L., 2017. Increasing AR by HIF-2alpha inhibitor (PT-2385) overcomes the side-effects of sorafenib by suppressing hepatocellular carcinoma invasion via alteration of pSTAT3, pAKT and pERK signals. Cell Death Dis. 8, e3095.

Yu, C.Y., Wang, Y.M., Li, N.M., Liu, G.S., Yang, S., Tang, G.T., He, D.X., Tan, X.W., Wei, H., 2014. In vitro and in vivo evaluation of pectin-based nanoparticles for hepatocellular carcinoma drug chemotherapy. Mol. Pharm. 11, 638–644.

Zhang, H., Hollis, C.P., Zhang, Q., Li, T., 2011. Preparation and antitumor study of camptothecin nanocrystals. Int. J. Pharm. 415, 293–300.

Zhang, S., Ong, C.N., Shen, H.M., 2004. Critical roles of intracellular thiols and calcium in parthenolide-induced apoptosis in human colorectal cancer cells. Cancer Lett. 208, 143–153.

Zhang, Z., Yang, L., Hou, J., Xia, X., Wang, J., Ning, Q., Jiang, S., 2018. Promising positive liver targeting delivery system based on arabinogalactan-anchored polymeric micelles of norcantharidin. Artif. Cells Nanomed. Biotechnol. 46, S630–S640.

Zhu, C., Zhaojun, X., Xiaohong, C., Fuhua, P., Xueqiang, H., Yanming, C., Qing, W., L., B. M., 2012. Artemisinin Attenuates Lipopolysaccharide-Stimulated Proinflammatory Responses by Inhibiting NF-κB Pathway in Microglia Cells. Plos One 7, e35125.

Zong, H., Sen, S., Zhang, G., Mu, C., Albayati, Z.F., Gorenstein, D.G., Liu, X., Ferrari, M., Crooks, P.A., Roboz, G.J., 2015. In vivo targeting of leukemia stem cells by directing parthenolide-loaded nanoparticles to the bone marrow niche. Leukemia 30, 1582.